Geophysical Research Letters

RESEARCH LETTER
10.1029/2019GL084089

Heavy Noble Gas Isotopes as New Constraints on the Ventilation of the Deep Ocean

Alan M. Seltzer[1], Frank J. Pavia[2], Jessica Ng[1], and Jeffrey P. Severinghaus[1]

[1]Scripps Institution of Oceanography, La Jolla, CA, USA, [2]Lamont-Doherty Earth Observatory, Palisades, NY, USA

Key Points:
- Ar, Kr, and Xe isotope ratios were measured in the deep North Pacific to investigate mechanisms of solubility disequilibrium
- Seawater solubility fractionation factors of heavy noble gas isotope ratios were determined, indicating a weak dependence on salinity
- Observed isotopic disequilibria point to incomplete cooling-driven diffusive gas uptake prior to deep-water formation

Supporting Information:
- Supporting Information S1
- Table S1

Correspondence to:
A. M. Seltzer,
aseltzer@ucsd.edu

Citation:
Seltzer, A. M., Pavia, F. J., Ng, J., & Severinghaus, J. P. (2019). Heavy noble gas isotopes as new constraints on the ventilation of the deep ocean. *Geophysical Research Letters*, *46*, 8926–8932. https://doi.org/10.1029/2019GL084089

Received 12 JUN 2019
Accepted 28 JUL 2019
Accepted article online 1 AUG 2019
Published online 8 AUG 2019

©2019. American Geophysical Union. All Rights Reserved.

Abstract Past studies of noble gas concentrations in the deep ocean have revealed widespread, several percent undersaturation of Ar, Kr, and Xe. However, the physical explanation for these disequilibria remains unclear. To gain insight into undersaturation set by deep-water formation, we measured heavy noble gas isotope and elemental ratios from the deep North Pacific using a new analytical technique. To our knowledge, these are the first high-precision seawater profiles of $^{38}Ar/^{36}Ar$ and Kr and Xe isotope ratios. To interpret isotopic disequilibria, we carried out a suite of laboratory experiments to measure solubility fractionation factors in seawater. In the deep North Pacific, we find undersaturation of heavy-to-light Ar and Kr isotope ratios, suggesting an important role for rapid cooling-driven, diffusive air-to-sea gas transport in setting the deep-ocean undersaturation of heavy noble gases. These isotope ratios represent promising new constraints for quantifying physical air-sea gas exchange processes, complementing noble gas concentration measurements.

Plain Language Summary The deep ocean inherits its dissolved gas content from exchange with the atmosphere at high latitudes and from biological and chemical processes. Noble gases, which are unaffected by biology and chemistry, are useful tools for understanding physical gas exchange. Past observations of dissolved noble gases throughout the deep ocean have revealed that Ar, Kr, and Xe concentrations fall below expected concentrations for water at solubility equilibrium with the atmosphere. However, a physical explanation for this well-documented undersaturation of noble gases remains unclear. Here we have measured the isotope ratios of Ar, Kr, and Xe in the deep North Pacific as new tools to investigate physical mechanisms of disequilibrium. Our findings suggest that rapid cooling and sinking of surface water at high latitudes, driving air-to-sea gas transport with insufficient time for equilibration, is a key process in setting the observed deep-ocean undersaturation of noble gases.

1. Introduction

Due to their chemical and biological inertness, dissolved noble gases in seawater are useful tools for disentangling physical from biogeochemical processes (Hamme et al., 2017; Stanley & Jenkins, 2013). Among other applications, noble gases have been used to constrain bubble injection (e.g., Emerson & Bushinsky, 2016; Stanley et al., 2009), diapycnal mixing rates (e.g., Ito et al., 2007), oxygen production (e.g., Spitzer & Jenkins, 1989), nutrient fluxes (e.g., Stanley et al., 2015), and the strength of the carbon solubility pump (Hamme et al., 2019; Nicholson et al., 2010). In the deep ocean, solubility disequilibria of noble gas concentrations display a globally consistent pattern (Hamme & Severinghaus, 2007; Jenkins et al., 2016; Loose et al., 2016): supersaturation of light, less soluble noble gases (He and Ne), and undersaturation of heavy, more soluble noble gases (Ar, Kr, and Xe). Deep-ocean Ne supersaturation is well understood to result from bubble injection during surface air-sea gas exchange or subsurface melting of glacial ice (Hamme & Emerson, 2002; Loose & Jenkins, 2014; Well & Roether, 2003). However, the cause of heavy noble gas undersaturation in the deep ocean remains less clear.

Two distinct physical explanations have been proposed, each of which concerns the strong temperature dependences of heavy noble gas solubilities. The first theory suggests that disequilibrium arises from incomplete air-to-sea transport of heavy noble gases during deep-water formation (Hamme et al., 2017; Hamme & Severinghaus, 2007; Nicholson et al., 2010). In this hypothesis, rapid wintertime cooling of the mixed layer increases gas solubilities, driving diffusive uptake by surface waters until they subduct, at which point gas exchange ceases and the signal of undersaturation is transported to the deep ocean. The second theory, which is most relevant to Antarctic sourced deep waters, suggests that disequilibrium is caused by

subsurface melting of glacial ice (Loose et al., 2016; Loose & Jenkins, 2014). In this hypothesis, the latent heat required for ice shelf melting is supplied by seawater, which cools and inherits gas from air bubbles liberated from melted ice, which completely dissolve under hydrostatic pressure. Undersaturation of Ar, Kr, and Xe therefore emerges because increases in solubility due to latent cooling are not fully compensated by the addition of gas from ice bubbles.

Here we explore the potential for isotope ratios of Ar, Kr, and Xe to provide constraints on mechanisms of deep-ocean heavy noble gas disequilibrium. While $^{40}Ar/^{36}Ar$ ratios in seawater have been measured once before at <1‰ precision (Nicholson et al., 2010), recent analytical developments have enabled high-precision measurement of dissolved $^{38}Ar/^{36}Ar$ and stable Kr and Xe isotope ratios in water (Seltzer et al., 2019). Ar, Kr, and Xe isotope ratios exhibit a range of sensitivities to bubble injection, cooling, and diffusive gas uptake as a result of their different solubility and kinetic fractionation factors (Seltzer et al., 2019). In this study, we analyzed Ar, Kr, and Xe isotope ratios at high precision in a small set of seawater samples collected from the deep North Pacific. We interpret our observations using a framework for isotopic fractionation that extends existing idealized models of bulk gas disequilibrium. This framework is informed by recent determinations of isotopic fractionation factors in freshwater (Seltzer et al., 2019) as well as new measurements of seawater isotopic solubility fractionation presented in this study.

2. Methods

2.1. Laboratory Determination of Isotopic Solubility Fractionation in Seawater

Solubility fractionation factors (α_{sol}) of Ar, Kr, and Xe isotope ratios in seawater were measured via closed-system laboratory equilibration experiments at Scripps Institution of Oceanography (SIO) in early 2019. α_{sol} is defined at a given temperature and salinity as

$$\alpha_{sol} = \frac{(H/L)_{diss}}{(H/L)_{gas}} \quad (1)$$

for a heavy isotope (H) and light isotope (L) at solubility equilibrium between the dissolved phase and gas phase at 100% relative humidity. In each experiment, 200–400 ml of seawater from the SIO pier (sterilized by ultraviolet light and a series of 100- and 25-μm filter bags) was equilibrated with a ~2-L noble gas headspace (either pure Ar or Ar-Xe/Ar-Kr mixtures) at ~1 atm for 36 hr at a constant temperature between ~2 and 25 °C following the closed system equilibration method of Seltzer et al. (2019). At the end of each experiment, a 2-ml headspace gas sample and 10- to 30-ml equilibrated seawater sample were collected. Dissolved gases from the seawater sample were quantitatively extracted by magnetic stirring under vacuum, and dissolved gas and headspace samples were each gettered using SAES Zr-Al sheets and Ti sponge at 900 °C for 1 hr. Isotope ratios in purified dissolved gas and headspace samples were analyzed on a Thermo-Finnigan MAT 253 mass spectrometer against a common reference gas. In total, 12 experiments were carried out: five each for Kr and Ar isotopes (at 34.6 ± 0.1 psu and 35.4 ± 0.1 psu, respectively), and two for Xe isotopes (at 36.8 ± 0.1 psu).

Figure 1 shows the results of these seawater solubility fractionation experiments as ε values (where $\varepsilon_{sol} \equiv \alpha_{sol} - 1$, in per mil) along with freshwater ε values (Seltzer et al., 2019). For Ar, Kr, and Xe at a given temperature, we find greater relative enrichment of heavy-to-light isotopes dissolved in seawater than in freshwater. This finding is consistent with $^{4}He/^{3}He$ solubility fractionation, which is also greater in seawater than in freshwater (Benson & Krause, 1980). In our experiments, the salinity effect on solubility fractionation is most pronounced for Ar isotopes and is insignificant for Kr and Xe isotopes. Surprisingly, the isotopic salinity effect does not appear to be strictly mass dependent, as the seawater-freshwater ε_{sol} difference for $^{38}Ar/^{36}Ar$ (two mass-unit difference) is similar in magnitude to that of $^{40}Ar/^{36}Ar$ (four mass-unit difference).

2.2. Seawater Sample Collection and Analysis

Seawater samples were collected from 10-L Niskin bottles on Hawaii Ocean Time-series (HOT) cruise 303 in June 2018. In total, 13 samples were collected at Station ALOHA (22.75°N 158°W) ranging from 250-m to 4.7-km depth. A mixed layer sample was collected from Station Kahe (21.34°N 158.27°W) at 6-m depth. Seawater was collected in preevacuated 2-L glass flasks following procedures described by Seltzer et al. (2019), based on a method for smaller dissolved gas samples (Hamme & Emerson, 2004).

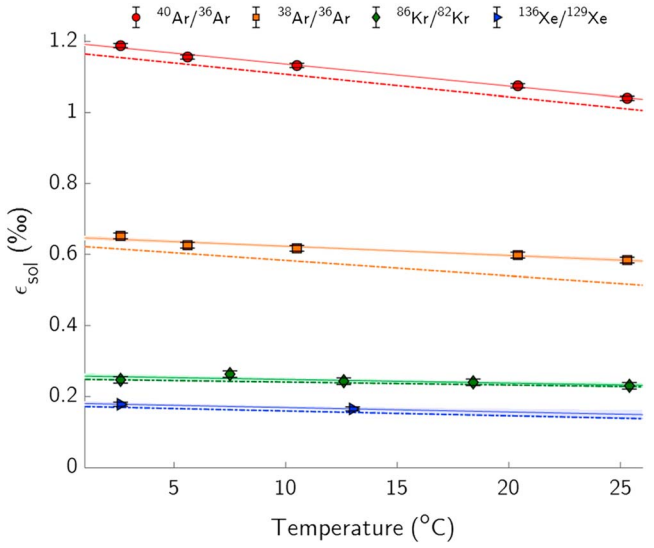

Figure 1. Ar, Kr, and Xe isotopic solubility fractionation in seawater (markers and solid lines: this study) and freshwater (dashed lines: Seltzer et al., 2019) versus temperature. The standard errors of seawater ϵ_{sol} values for the isotope ratios considered in this study range from ±4 per meg for $^{40}Ar/^{36}Ar$ to ±7 per meg for $^{86}Kr/^{82}Kr$. Error bars indicate ±1–σ and ±1–standard error ranges of individual experiments and temperature trend lines, respectively.

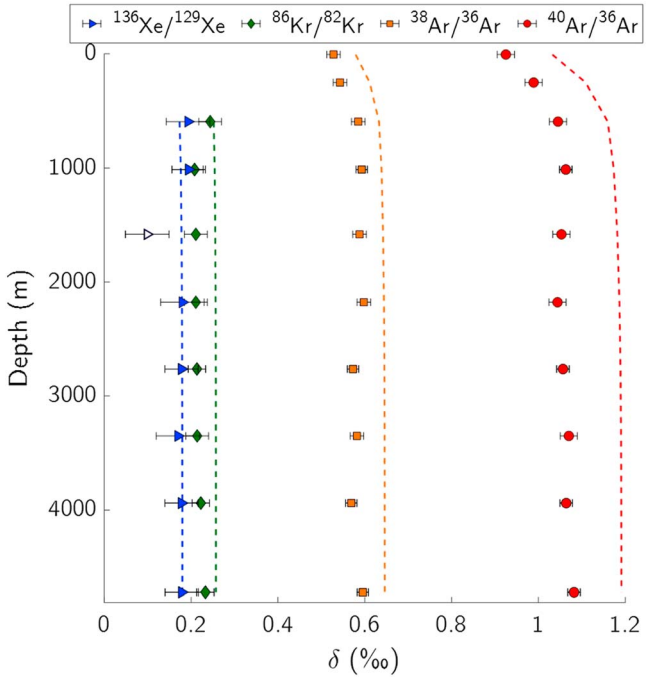

Figure 2. Measured HOT 303 profiles of dissolved Ar, Kr, and Xe isotope ratios, relative to atmospheric air (in ‰). Error bars indicate standard errors of depth-mean values. An outlier Xe isotope measurement at ~1.6 km is shaded white. Dashed lines indicate our measured seawater solubility equilibria (ϵ_{sol}).

At SIO, dissolved gases were quantitatively extracted by sparging with ultrahigh purity helium gas in a recirculating loop, trapping all nonhelium gases in a stainless-steel dip tube immersed in liquid helium (Seltzer et al., 2019). Extracted gases were then purified by gettering with SAES Zr-Al sheets at 900 °C for 130 min. For all samples collected below 500 m, stable isotope and elemental ratios of Ar, Kr, and Xe were analyzed on a Thermo-Finnigan MAT 253. Due to insufficient gas content, only Ar isotopes and elemental ratios were measured in the shallowest two samples at 6 and 250 m, which were 26.8 and 14.5 °C, respectively. Prior to mass spectrometry, dissolved Ar concentrations were measured by manometry.

To interpret HOT 303 measurements, we report dissolved gas ratios and concentrations relative to solubility equilibrium at 1 atm and 100% relative humidity using the newly determined noble gas solubility functions from Jenkins et al. (2019) and the isotopic solubility fractionation factors in seawater determined in this study. These solubility anomalies are defined for gas concentrations, ΔC, and ratios, $\Delta\delta$, as follows:

$$\Delta C \equiv \frac{C}{C_{eq}(S,\theta)} - 1 \quad (2)$$

$$\Delta\delta \equiv \frac{R/R_{atm}}{\alpha_{sol}(S,T)} - 1 \quad (3)$$

where C is a measured dissolved gas concentration (μmol/kg), C_{eq} is a concentration at solubility equilibrium at potential temperature θ (°C) and salinity S (psu) assuming equilibration with unfractionated atmospheric air at 1 atm pressure and 100% relative humidity. In equation (3), R is a gas or isotope ratio and R_{atm} is that ratio in the well-mixed atmosphere.

In this study, measured gas ratios are reported either as (a) δ values referenced to atmospheric air, or (b) $\Delta\delta$ values referenced to dissolved ratios at solubility equilibrium. For each of these variables, we account for uncertainties based on measurement reproducibility, error in systematic mass spectrometry and extraction system corrections, error in atmospheric reference gas analysis, and uncertainty in α_{sol} (which only affects $\Delta\delta$). Details are provided in the supporting information section S1.

3. Observations From the Deep North Pacific (HOT 303, June 2018)

Figure 2 shows measured depth profiles of HOT 303 Ar, Kr, and Xe isotope ratios beside solubility equilibrium values. Across eight samples collected from the deep ocean (defined hereafter as below 2,000 m), we observe mean $\delta^{40}/_{36}Ar$, $\delta^{38}/_{36}Ar$, $\delta^{86}/_{82}Kr$, and $\delta^{136}/_{129}Xe$ of 1.065 ± 0.013‰, 0.582 ± 0.013‰, 0.220 ± 0.009‰, and 0.177 ± 0.003‰ (±1σ). Replicate 2-L samples were collected at ~1,000, 2,800, 4,000, and 4,700 m, and single samples were collected at all other depths. Both $\delta^{40}/_{36}Ar$ and $\delta^{38}/_{36}Ar$ increase from the surface to deep ocean, and Kr and Xe isotope ratios are relatively constant with depth from ~600 to 4,700 m.

Solubility anomalies of measured isotope and gas ratios, Δδ and ΔKr/Ar, are shown in Figure 3 as a function of depth. In the deep ocean, we find that Ar and Kr isotope ratios fall significantly below solubility equilibrium (at the 95% confidence level). Mean $\Delta\delta^{40}/_{36}Ar$, $\Delta\delta^{38}/_{36}Ar$, $\Delta\delta^{86}/_{82}Kr$ below 2000 m are −125 ± 10 per meg, −64 ± 13 per meg, −37 ± 15 per

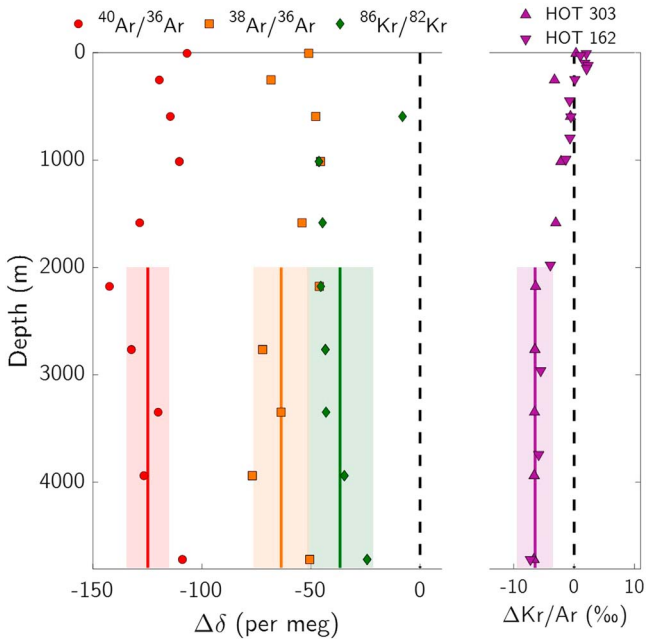

Figure 3. Solubility disequilibria for measured stable isotope ratios (left panel) and Kr/Ar ratios (right panel). Solid lines and shaded regions indicate mean and standard error of deep-ocean (>2,000 m) disequilibria. All measurements are from HOT 303, except for the HOT 162 Kr/Ar data (Hamme & Severinghaus, 2007).

meg (±1 standard error), respectively, where 1 per meg = 0.001‰ = 0.0001%. Deep-ocean mean $\Delta\delta^{136}/_{129}$Xe is −2 ± 25 per meg. While uncertainties prevent meaningful interpretation of this small value, we suggest that future gains in analytical precision and large-volume sampling campaigns could resolve Xe isotopic disequilibria at the single per meg level.

The ΔKr/Ar determined in this study closely matches ΔKr/Ar measured from an August 2004 HOT cruise (HOT 162, Hamme & Severinghaus, 2007). In the deep-ocean, mean HOT 303 and HOT 162 ΔKr/Ar are −6.6‰ and −6.2‰, respectively, relative to recently redetermined Kr and Ar solubilities in seawater (Jenkins et al., 2019). In the surface ocean, we observe ΔKr/Ar near zero (~0.3‰) and negative $\Delta\delta^{40}/_{36}$Ar and $\Delta\delta^{38}/_{36}$Ar (−107 ± 20 per meg and −51 ± 20 per meg, respectively). The surface and intermediate ocean data will be discussed in a separate study. However, here we note that although $\Delta\delta^{40}/_{36}$Ar appears similar in the warm surface ocean and cold deep ocean, the physical mechanisms driving isotopic disequilibrium in the warm surface ocean are distinct from the deep ocean (supporting information section S2).

4. Interpreting Solubility Disequilibria: A Unified Framework for Dissolved Gas Concentrations (ΔC) and Ratios ($\Delta\delta$)

To gain insight into processes setting the observed isotopic disequilibria in the deep North Pacific, we have extended existing idealized equations for bulk gas disequilibria, ΔC, to gas ratios. Prior studies have proposed linear combinations of ΔC for individual disequilibrium mechanisms, each acting on initially air-saturated seawater at 100% relative humidity and 1 atm pressure. These processes include warming or cooling (Hamme et al., 2017; Hamme & Emerson, 2002; Hamme & Severinghaus, 2007), bubble injection (Emerson & Bushinsky, 2016; Liang et al., 2013; Nicholson et al., 2011; Stanley et al., 2009), submarine melting of glacial ice (Loose & Jenkins, 2014), diapycnal mixing (Ito et al., 2007; Ito & Deutsch, 2006; Spitzer & Jenkins, 1989), and other processes both for cases of no gas exchange (e.g., in the ocean interior or under sea ice) or diffusive air-sea gas exchange such that a quasi steady state is reached at which ΔC is temporally constant. To extend equations for ΔC to $\Delta\delta$, we make use of an alternate definition for $\Delta\delta$ for a ratio of gases or isotopes i and j:

$$\Delta\delta = \frac{C_i/C_{i,\mathrm{eq}}}{C_j/C_{\mathrm{j,eq}}} - 1 = \frac{\Delta C_i + 1}{\Delta C_j + 1} - 1 \tag{4}$$

One key benefit of considering disequilibrium of ratios rather than concentrations is that ratios are unaffected by barometric pressure, which can be several percent below 1 atm in high-latitude regions of deep-water formation (Loose et al., 2016; Well & Roether, 2003).

Figure 4 shows the influence of seven distinct processes on $\Delta\delta^{86}/_{82}$Kr, $\Delta\delta^{40}/_{36}$Ar, and on ΔKr/Ar, and ΔNe/Ar. (Note: in the supporting information section S3, we define ΔC for each process formally.) The disequilibria modeled in Figure 4 result from the following processes acting on an initially air-saturated 2-°C, 35-psu, 100-m mixed layer:

1. cooling and warming of 2 °C without air-sea gas exchange
2. constant cooling of 1.2 °C/month inducing a quasi steady state diffusive air-to-gas flux to maintain constant ΔC under 10 m/s winds (with gas exchange parameterized by the Wanninkhof, 2014)
3. the addition of 0.5% glacial meltwater by subsurface ice-shelf melting using parameters given in Loose et al. (2016) and assuming a 100-m firn thickness
4. small bubble dissolution (0.025 mol_{air}/m^3) without air-sea diffusive gas exchange
5. steady state small bubble dissolution (0.125 $mol_{air}\cdot m^{-2}\cdot day^{-1}$) balanced by diffusive reexchange with the atmosphere

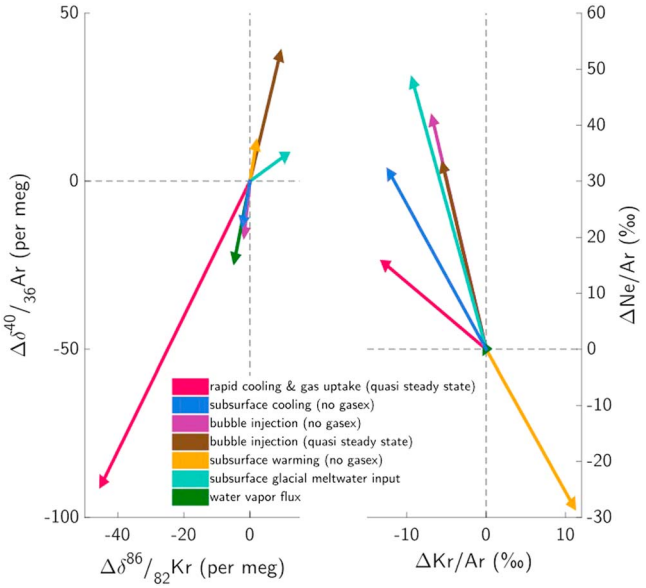

Figure 4. Idealized expectations for isotope and elemental ratio disequilibria resulting from seven processes detailed in section 4. For each process, an initially air-saturated ($\Delta C = 0$, $\Delta\delta = 0$) 100-m mixed layer at 2 °C and 35 psu is assumed.

6. kinetic fractionation of atmospheric air ratios in the molecular boundary layer above the air-sea interface due to steady state diffusion against the upward flux of water vapor.

The last process above, hereafter "water vapor flux fractionation," is a ternary fractionation that arises from differences in binary diffusivities of two gases or isotopes against water vapor (Severinghaus et al., 1996). Because a steady state gradient exists between the mole fractions of water vapor at the air-sea interface (100% relative humidity) and in the turbulently mixed air above (~80% relative humidity), an inverse mole fraction gradient exists for all other dry air constituents, driving steady state diffusion and inducing kinetic fractionation (Figure S2). Because this effect scales with saturation vapor pressure, it can be significant above warm water. For example, at 26.5 °C and 80% relative humidity it causes steady state fractionation of −115 per meg and −60 per meg for $\delta^{40}/_{36}$Ar and $\delta^{38}/_{36}$Ar, respectively, close to our observations of −107 ± 20 per meg and −51 ± 20 per meg in the mixed layer at Station Kahe. In contrast, above cold water, water vapor flux fractionation is greatly reduced and therefore is only a minor contributor to isotopic fractionation in the cold, high-latitude-sourced deep ocean.

Four of the processes shown in Figure 4 yield negative ΔKr/Ar and positive ΔNe/Ar, consistent with global deep-ocean observations (Hamme et al., 2017; Hamme & Severinghaus, 2007; Jenkins et al., 2016; Loose et al., 2016). Of these processes, only one causes substantially negative Δδ for Ar and Kr isotope ratios: rapid cooling-induced diffusive gas uptake. Cooling of the mixed layer drives air-to-sea diffusion, inducing kinetic fractionation of isotope ratios (negative Δδ) due to the faster diffusivities of light isotopes. Critically important is the difference between cooling-driven gas uptake and glacial meltwater input, the two leading hypotheses for the undersaturation of heavy noble gases in the deep ocean. Whereas both processes yield ~ −1% ΔKr/Ar, consistent with observations, cooling-driven diffusive gas uptake and glacial meltwater input fractionate isotope ratios in diverging directions (e.g., −90 per meg vs. +38 per meg for $\delta^{40}/_{36}$Ar). Glacial meltwater input causes positive Δδ because gravitational enrichment of firn air (Schwander, 1989) prior to occlusion in bubbles fractionates $\delta^{40}/_{36}$Ar and $\delta^{86}/_{82}$Kr (~2‰ over a 100-m firn column) more strongly than does solubility fractionation (ε_{sol} ~ 1.2‰ and 0.25‰, respectively). The deep HOT data therefore suggest an important role for rapid cooling-driven diffusive gas uptake in setting the undersaturation of heavy noble gases in the deep ocean.

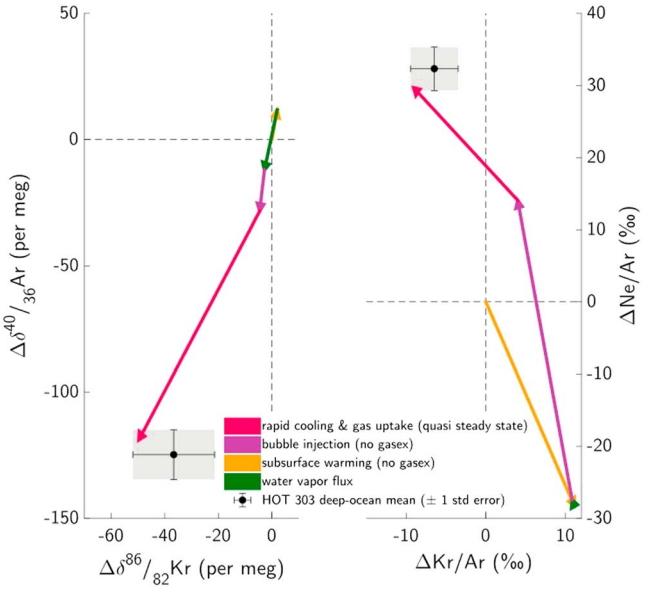

Figure 5. Possible combination of disequilibrium mechanisms that may explain HOT 303 deep ocean observations. In this scenario, rapid cooling (1.2 °C/month) of the surface ocean occurs after the deepening of a shallow summer mixed layer and entrainment of radiatively warmed (by 2 °C) water. Injection and complete dissolution of air bubbles (0.025 mol_{air}/m^3) and diffusive gas uptake lead to fractionation of isotope and elemental ratios prior to subduction.

In Figure 5, we present a possible combination of processes that may simultaneously explain these isotopic observations as well as previous Kr/Ar and Ne/Ar measurements in the deep ocean at Station ALOHA (Hamme & Severinghaus, 2007). In this deep-water formation scenario, which most resembles North Atlantic-like deep convection, mixed layer deepening during late fall first entrains radiatively warmed water at the base of the shallower summer mixed layer, leading to supersaturation. Superimposed on this supersaturation is a small, steady state water vapor flux fractionation in the cold air-side molecular sublayer. Then, as the surface ocean rapidly cools, noble gases are taken up both by bubble-mediated and diffusive exchange before the surface layer sinks and loses contact with the atmosphere, locking in signals of kinetic isotopic fractionation and bulk undersaturation. We assume here that all bubbles completely dissolve; however, we note that partial dissolution of bubbles

(e.g., Keeling, 1993) may be another source of kinetic fractionation. Importantly, subsurface melting of glacial ice is not required in this scenario.

We suggest that future observations of deep-ocean noble gas isotopic disequilibria over a wide spatial range may reveal differences in the relative importance of the North Atlantic and Southern Oceans in ventilating the deep ocean (Gebbie et al., 2010; Johnson, 2008; Khatiwala et al., 2012; Rae & Broecker, 2018) due to their considerably different formation and gas exchange processes, which likely lead to different fingerprints of noble gas elemental and isotopic fractionation. Whereas gas exchange during deep-water formation in the North Atlantic is fairly well characterized (e.g., Hamme et al., 2017; Wolf et al., 2018), the physical mechanisms of Antarctic deep-water formation and their impact on gas exchange are poorly understood. Future measurements of noble gas isotopes in recently formed Antarctic bottom waters may thus shed light on gas exchange processes and improve predictions of the physical components of solubility disequilibrium for gases such as O_2 and CO_2. Climate model simulations have been used to understand and predict past and future changes in global air-sea transport of O_2 and CO_2 (Ito & Follows, 2013; Khatiwala et al., 2019). Precise knowledge of deep-ocean noble gas isotopic disequilibria provides a benchmark to evaluate climate model simulations of air-sea gas transport during deep-water formation.

5. Conclusions

In this study, we introduced a framework for investigating the influence of physical gas-exchange mechanisms during deep-water formation on the isotopic composition of heavy noble gases. We carried out experiments to determine isotopic solubility fractionation factors in seawater and discovered slightly greater isotopic discrimination in seawater than in freshwater. To explore mechanisms of inert gas disequilibrium caused by deep-water formation, we collected and analyzed a small set of samples from the deep North Pacific and found undersaturation of heavy-to-light Ar and Kr isotope ratios, which point to the importance of rapid cooling-driven diffusive gas uptake. We suggest that future measurements of Ar, Kr, and Xe isotope ratios, with moderate gains in analytical precision and paired with measurements of He, Ne, Ar, Kr, and Xe, will provide additional sensitive constraints for quantifying physical drivers of deep-ocean ventilation. Future measurements may better inform the saturation and transport of biogeochemically important gases like O_2 and CO_2 as well as ventilation age tracers like CFCs and SF_6.

Acknowledgments
We thank Dan Sadler and the captains and crew of R/V *Ka'imikai-O-Kanaloa* for enabling our seawater collection, Roberta Hamme for sampling advice, Manuel Belmonte and May-Linn Paulsen for salinity measurements, and Bill Paplawski, Martin Tresguerres, Steve Emerson, Susan Becker, Adam Cox, and Ross Beaudette for technical support and equipment loans. This work was supported by two NSF Graduate Research Fellowships, a Geological Society of America Graduate Research Award, the Shepard Foundation, Hawaiian Airlines, and NSF award EAR-1702704. All data are available in the supporting information.

References

Benson, B. B., & Krause, D. (1980). Isotopic fractionation of helium during solution: A probe for the liquid state. *Journal of Solution Chemistry*, *9*(12), 895–909. https://doi.org/10.1007/BF00646402

Emerson, S., & Bushinsky, S. (2016). The role of bubbles during air-sea gas exchange. *Journal of Geophysical Research: Oceans*, *121*, 4360–4376. https://doi.org/10.1002/2016JC011744

Gebbie, G., Huybers, P., Gebbie, G., & Huybers, P. (2010). Total matrix intercomparison: A method for determining the geometry of water-mass pathways. *Journal of Physical Oceanography*, *40*(8), 1710–1728. https://doi.org/10.1175/2010JPO4272.1

Hamme, R. C., & Emerson, S. R. (2002). Mechanisms controlling the global oceanic distribution of the inert gases argon, nitrogen and neon. *Geophysical Research Letters*, *29*(23), 2120. https://doi.org/10.1029/2002GL015273

Hamme, R. C., & Emerson, S. R. (2004). Measurement of dissolved neon by isotope dilution using a quadrupole mass spectrometer. *Marine Chemistry*, *91*(1–4), 53–64. https://doi.org/10.1016/j.marchem.2004.05.001

Hamme, R. C., Emerson, S. R., Severinghaus, J. P., Long, M. C., & Yashayaev, I. (2017). Using noble gas measurements to derive air-sea process information and predict physical gas saturations. *Geophysical Research Letters*, *44*, 9901–9909. https://doi.org/10.1002/2017GL075123

Hamme, R. C., Nicholson, D. P., Jenkins, W. J., & Emerson, S. R. (2019). Using noble gases to assess the ocean's carbon pumps. *Annual Review of Marine Science*, *11*(1), 75–103. https://doi.org/10.1146/annurev-marine-121916-063604

Hamme, R. C., & Severinghaus, J. P. (2007). Trace gas disequilibria during deep-water formation. *Deep Sea Research Part I: Oceanographic Research Papers*, *54*(6), 939–950. https://doi.org/10.1016/j.dsr.2007.03.008

Ito, T., & Deutsch, C. (2006). Understanding the saturation state of argon in the thermocline: The role of air-sea gas exchange and diapycnal mixing. *Global Biogeochemical Cycles*, *20*, GB3019. https://doi.org/10.1029/2005GB002655

Ito, T., Deutsch, C., Emerson, S., & Hamme, R. C. (2007). Impact of diapycnal mixing on the saturation state of argon in the subtropical North Pacific. *Geophysical Research Letters*, *34*, L09602. https://doi.org/10.1029/2006GL029209

Ito, T., & Follows, M. J. (2013). Air-sea disequilibrium of carbon dioxide enhances the biological carbon sequestration in the Southern Ocean. *Global Biogeochemical Cycles*, *27*, 1129–1138. https://doi.org/10.1002/2013GB004682

Jenkins, W. J., Lott, D. E., & Cahill, K. L. (2019). A determination of atmospheric helium, neon, argon, krypton, and xenon solubility concentrations in water and seawater. *Marine Chemistry*, *211*, 94–107. https://doi.org/10.1016/J.MARCHEM.2019.03.007

Jenkins, W. J., Lott, D. E., German, C. R., Cahill, K. L., Goudreau, J., & Longworth, B. (2016). The deep distributions of helium isotopes, radiocarbon, and noble gases along the U.S. GEOTRACES East Pacific Zonal Transect (GP16). *Marine Chemistry*, *201*, 167–182. https://doi.org/10.1016/j.marchem.2017.03.009

Johnson, G. C. (2008). Quantifying Antarctic bottom water and North Atlantic deep water volumes. *Journal of Geophysical Research*, *113*, C05027. https://doi.org/10.1029/2007JC004477

Keeling, R. F. (1993). On the role of large bubbles in air-sea gas exchange and supersaturation in the ocean. *Journal of Marine Research*, *51*(2), 237–271. https://doi.org/10.1357/0022240933223800

Khatiwala, S., Primeau, F., & Holzer, M. (2012). Ventilation of the deep ocean constrained with tracer observations and implications for radiocarbon estimates of ideal mean age. *Earth and Planetary Science Letters*, *325-326*, 116–125. https://doi.org/10.1016/J.EPSL.2012.01.038

Khatiwala, S., Schmittner, A., & Muglia, J. (2019). Air-sea disequilibrium enhances ocean carbon storage during glacial periods. *Science Advances*, *5*(6), eaaw4981. https://doi.org/10.1126/sciadv.aaw4981

Liang, J.-H., Deutsch, C., McWilliams, J. C., Baschek, B., Sullivan, P. P., & Chiba, D. (2013). Parameterizing bubble-mediated air-sea gas exchange and its effect on ocean ventilation. *Global Biogeochemical Cycles*, *27*, 894–905. https://doi.org/10.1002/gbc.20080

Loose, B., & Jenkins, W. J. (2014). The five stable noble gases are sensitive unambiguous tracers of glacial meltwater. *Geophysical Research Letters*, *41*, 2835–2841. https://doi.org/10.1002/2013GL058804

Loose, B., Jenkins, W. J., Moriarty, R., Brown, P., Jullion, L., Naveira Garabato, A. C., et al. (2016). Estimating the recharge properties of the deep ocean using noble gases and helium isotopes. *Journal of Geophysical Research: Oceans*, *121*, 5959–5979. https://doi.org/10.1002/2016JC011809

Nicholson, D., Emerson, S., Caillon, N., Jouzel, J., & Hamme, R. C. (2010). Constraining ventilation during deepwater formation using deep ocean measurements of the dissolved gas ratios $^{40}Ar/^{36}Ar$, N_2/Ar, and Kr/Ar. *Journal of Geophysical Research*, *115*, C11015. https://doi.org/10.1029/2010JC006152

Nicholson, D. P., Emerson, S. R., & Khatiwala, S. (2011). An inverse approach to estimate bubble-mediated air-sea gas flux from inert gas measurements. In S. Komori, & R. Karose (Eds.), *Proceedings on the 6th International Symposium on Gas Transfer at Water Surfaces* (pp. 223–237). Kyoto, Japan. Retrieved from: Kyoto Univ. Press. https://pdfs.semanticscholar.org/021d/45190e104eaa02ff-b0e37b96556395ca6442.pdf?_ga=2.128534155.648866189.1555369155-1227961956.1555369155

Rae, J. W. B., & Broecker, W. (2018). What fraction of the Pacific and Indian Oceans' deep water is formed in the Southern Ocean? *Biogeosciences*, *15*(12), 3779–3794. https://doi.org/10.5194/bg-15-3779-2018

Schwander, J. (1989). The transformation of snow to ice and the occlusion of gases. In H. Oeschger, & C. C. Langway (Eds.), *The environmental record in glaciers and ice sheets*, (pp. 53–67). New York: Wiley.

Seltzer, A. M., Ng, J., & Severinghaus, J. P. (2019). Precise determination of Ar, Kr and Xe isotopic fractionation due to diffusion and dissolution in fresh water. *Earth and Planetary Science Letters*, *514*, 156–165. https://doi.org/10.1016/J.EPSL.2019.03.008

Severinghaus, J. P., Bender, M. L., Keeling, R. F., & Broecker, W. S. (1996). Fractionation of soil gases by diffusion of water vapor, gravitational settling, and thermal diffusion. *Geochimica et Cosmochimica Acta*, *60*(6), 1005–1018. https://doi.org/10.1016/0016-7037(96)00011-7

Spitzer, W. S., & Jenkins, W. J. (1989). Rates of vertical mixing, gas exchange and new production: Estimates from seasonal gas cycles in the upper ocean near Bermuda. *Journal of Marine Research*, *47*(1), 169–196. https://doi.org/10.1357/002224089785076370

Stanley, R. H. R., & Jenkins, W. (2013). Noble gases in seawater as tracers for physical and biogeochemical ocean processes. In *The Noble Gases as Geochemical Tracers*, (pp. 55–79). Berlin Heidelberg: Springer. https://doi.org/10.1007/978-3-642-28836-4_4

Stanley, R. H. R., Jenkins, W. J., Doney, S. C., & Lott, D. E. (2015). The 3 He flux gauge in the Sargasso Sea: A determination of physical nutrient fluxes to the euphotic zone at the Bermuda Atlantic Time-series Site. *Biogeosciences*, *12*(17), 5199–5210. https://doi.org/10.5194/bg-12-5199-2015

Stanley, R. H. R., Jenkins, W. J., Lott, D. E., & Doney, S. C. (2009). Noble gas constraints on air-sea gas exchange and bubble fluxes. *Journal of Geophysical Research*, *114*, C11020. https://doi.org/10.1029/2009JC005396

Wanninkhof, R. (2014). Relationship between wind speed and gas exchange over the ocean revisited. *Limnology and Oceanography: Methods*, *12*(6), 351–362. https://doi.org/10.4319/lom.2014.12.351

Well, R., & Roether, W. (2003). Neon distribution in South Atlantic and South Pacific waters. *Deep Sea Research Part I: Oceanographic Research Papers*, *50*(6), 721–735. https://doi.org/10.1016/S0967-0637(03)00058-X

Wolf, M. K., Hamme, R. C., Gilbert, D., Yashayaev, I., & Thierry, V. (2018). Oxygen saturation surrounding deep water formation events in the Labrador Sea from Argo-O_2 data. *Global Biogeochemical Cycles*, *32*, 635–653. https://doi.org/10.1002/2017GB005829